Progress In Electromagnetics Research, PIER 101, 63–74, 2010

WIRELESS COMMUNICATION IN BOXES WITH METALLIC ENCLOSURE BASED ON TIME-REVERSAL ULTRA-WIDEBAND TECHNIQUE: A FULL-WAVE NUMERICAL STUDY

H. Q. Zhai, S. Y. Jung, and M. Y. Lu

Department of Electrical Engineering
The University of Texas at Arlington
Arlington, TX 76019, USA

Abstract—In this paper, two full-wave simulators (one using finite difference time domain method and the other the method of moments) are developed, in order to analyze wireless communication in boxes with metallic enclosure based on time-reversal ultra-wideband (TR-UWB) technique. Impedance boundary conditions are exploited to model realistic metallic walls; and parallel computing is applied to relieve high computational resources requirements. Focusing in both space and time is exhibited by numerical results in arbitrarily shaped metallic boxes, which demonstrates the feasibility of TR-UWB communication in metallic boxes.

1. INTRODUCTION

Boxes with metallic enclosure embody various realistic environments in which wireless communication plays important roles. For instance, in space stations wireless communication offers substantial movement freedom to the astronauts [1]. As another example, sensors in a modern automobile require cables with 1000 meters length and 50 kg weight; and it is beneficial to replace these wired connections by wireless ones [2]. In boxes with metallic enclosure, multiple reflections due to surrounding reflective walls result in extremely dispersive channels, which in turn makes wireless communication difficult [3]. In recent years, time-reversal ultra-wideband (TR-UWB) technique has been proved to have excellent potential to resolve the channel dispersion issue [4, 5]. Unlike traditional equalization methods (such as RAKE [6]) that tackle dispersive channels directly, TR-UWB takes advantage

Corresponding author: H. Q. Zhai (huiqing@uta.edu).

of channel reciprocity and round-trip propagation to compensate the channels "indirectly." TR-UWB requires little channel estimation and it focuses electromagnetic waves dispersed in both space and time. Moreover, the more complex the channel is, the better performance TR-UWB has [7]. Therefore, TR-UWB is expected to be a close-to-optimal solution to wireless communication in extremely complex environments like metallic boxes.

However, the complex electromagnetic propagation channels in boxes with metallic enclosure make accurate modeling of TR-UWB communication challenging. If carried out in the frequency domain, the modeling unavoidably encounters matrices with poor condition numbers due to the enclosed configurations. If time domain simulators are applied, rich multiple reflections must be precisely tracked for a long time. In the past, radio waves in enclosed-space were analyzed by ray-tracing method, which approximates radio-frequency waves by optical rays [8]. In this paper, TR-UWB communication in arbitrarily-shaped boxes with metallic enclosure is rigorously analyzed using full-wave simulations. To be specific, two Maxwell's equations solvers, one based on finite difference time domain (FDTD) and the other the method of moments (MoM), are developed to track electromagnetic wave propagation in the boxes. Impedance boundary condition (IBC) is exploited to model realistic metallic walls [9]. The MoM matrices are solved using LU decomposition instead of iterative solvers, to mitigate the effects of poor condition number. In order to relieve high computational resources requirements, these simulators are implemented on parallel cluster computers. Results from FDTD and MoM simulators match one another; and they show focusing in both space and time after time-reversal and round-trip propagation operations are carried out onto UWB impulses, which demonstrates the feasibility of TR-UWB communication in boxes with metallic enclosure.

This paper is organized as follows. In Section 2, numerical methods to analyze TR-UWB communication in metallic boxes are described. Some numerical results are presented in Section 3. Finally, Section 4 relates to our conclusions.

2. NUMERICAL MODELING OF TR-UWB IN METALLIC BOXES

A major distinction between TR-UWB and conventional communication schemes is that TR-UWB involves round-trip (backward and forward) propagation. *Backward propagation* is depicted in Figure 1(a): the receiver (RX) transmits narrow impulses; due to multi-path in the

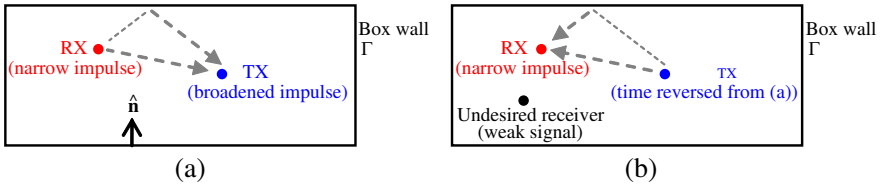

Figure 1. Illustration of TR-UWB communication in metallic boxes. (a) Backward propagation (from RX to TX). (b) Forward propagation (from TX to RX).

box, the impulses get broadened in time when they reach the transmitter (TX). Next, the broadened impulses are time reversed at the TX, and the time-reversed impulses are considered "carriers." When these carriers are transmitted by the TX (*forward propagation* in Figure 1(b)), narrow impulses result at the RX (temporal compression), and receptions at any undesired receivers are weaker than that at the RX (spatial focusing), as long as the channel between TX and RX is reciprocal [5]. As a consequence, when the TX modulates the carriers, the RX does not suffer from severe inter-symbol or co-channel interferences.

It is challenging to simulate electromagnetic waves' propagation in metallic boxes, because of two major reasons. The first reason is related to the modeling of box walls. If the box walls are made of perfect conductor, signals in the box would keep being bounced back and forth for infinite number of times. In this paper, box walls are assumed to be realistic metal and they are modeled by IBCs. Due to the usage of IBC, the signals are attenuated (though slowly) by the loss of imperfect conductor. The second reason is high computational resources requirement. If the simulation is carried out in time domain, many time steps are called for to track the long waveforms. Frequency domain simulation has similar problems: small frequency step size must be applied to the problem configurations illustrated in Figure 1, especially around resonant frequencies. In this paper, parallel computing is resorted to relieve the high computational cost. Specifically, two parallel Maxwell's equations solvers are developed on cluster computers with distributed memory. One of them is a time domain solver based on FDTD, and the other one is based on MoM executed in frequency domain. In the rest of this section, full-wave simulations of TR-UWB communication in metallic boxes using parallel FDTD and MoM are described in detail.

In both FDTD and MoM simulators, box walls are modeled by Leontovich IBC [10]:

$$\hat{\mathbf{n}}(\mathbf{r}) \times \hat{\mathbf{n}}(\mathbf{r}) \times \mathbf{E}(\mathbf{r}, t) = -R_s(t) * \hat{\mathbf{n}}(\mathbf{r}) \times \mathbf{H}(\mathbf{r}, t), \quad \mathbf{r} \in \Gamma. \tag{1}$$

In the above, "Γ" denotes box boundary; $\hat{\mathbf{n}}$ is unit direction normal to Γ (Figure 1); $R_s(t)$ is the surface resistance in time domain and it is the inverse Fourier transform of $Z_s(\omega) = \sqrt{j\omega\mu/(\sigma + j\omega\varepsilon)}$, which is the surface impedance in frequency domain; $j = \sqrt{-1}$; ε, μ, and σ are permittivity, permeability, and conductivity of the box wall, respectively; and "*" denotes temporal convolution. In this paper, it is assumed that the box wall is made of good metal thus $\sigma \gg \omega\varepsilon$. As a result,

$$Z_s(\omega) = \sqrt{\frac{j\omega\mu}{\sigma + j\omega\varepsilon}} \approx \sqrt{\frac{j\omega\mu}{\sigma}}, \tag{2}$$

and

$$R_s(t) = \frac{1}{\pi}\mathrm{Re}\left\{\int_0^\infty \sqrt{\frac{j\omega\mu}{\sigma}} e^{j\omega t} d\omega\right\} = \frac{d}{dt}\left(\sqrt{\frac{\mu}{\sigma\pi}}\frac{U(t)}{\sqrt{t}}\right), \tag{3}$$

where operator "Re" takes the real part of its argument, and $U(t)$ is Heaviside step function.

When FDTD is applied to analyze TR-UWB communication in metallic boxes in this paper, regular Yee cells are used to discretize the problem geometry [11]. During spatial discritization, there are only tangential electric field samples and normal magnetic field samples over Γ, as illustrated in Figure 2 (In Figure 2, Γ is marked by the shaded surfaces). Regular update equations for Yee cells are utilized when no samples on Γ are involved. Incorporation of IBC into FDTD update equations for samples next to Γ is discussed in the below. Suppose y

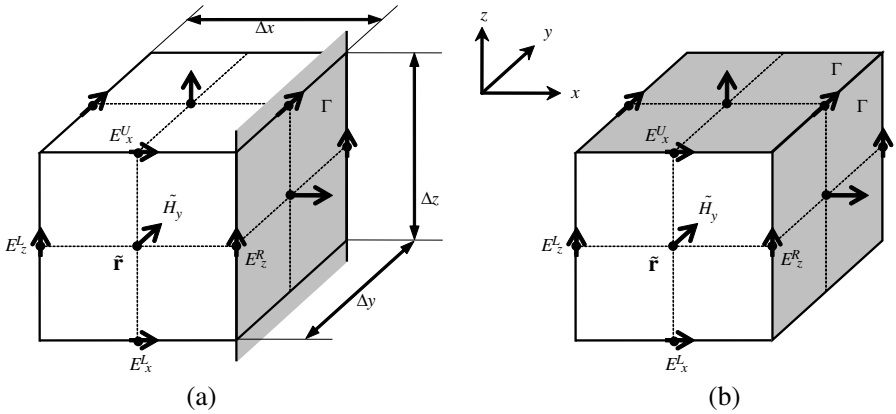

Figure 2. Illustration of FDTD simulator. (a) Next to boundary but not next to boundary edge. (b) Next to boundary edge.

component of magnetic field is sampled at location $\tilde{\mathbf{r}}$ as $\tilde{H}_y(t)$, its time derivative can be approximated by four electric field samples around it (including upper E_x, lower E_x, left E_z, and right E_z), as illustrated by Figure 2:

$$-\tilde{\mu}\frac{d\tilde{H}_y(t)}{dt} = \frac{E_x^U(t) - E_x^L(t)}{\Delta z} + \frac{E_z^L(t) - E_z^R(t)}{\Delta x}, \tag{4}$$

where $\tilde{\mu}$ is the permeability at location $\tilde{\mathbf{r}}$, and Δx, Δy, and Δz are the side lengths of Yee cells. In the situation shown in Figure 2(a), E_z^R is located on Γ, hence it is related to $\tilde{H}_y$ through (1). Specifically,

$$E_z^R(t) = -\tilde{H}_y(t) * R_s(t) = -\left\{\left(\frac{d\tilde{H}_y(t)}{dt}\right) * \left(\sqrt{\frac{\mu}{\sigma\pi}}\frac{U(t)}{\sqrt{t}}\right)\right\}. \tag{5}$$

Suppose magnetic fields are sampled in time at $(n-0.5)\Delta t$, and electric fields are sampled in time at $n\Delta t$, $n = 1, 2, 3, \ldots$, where Δt is the time step size in FDTD. Time derivative of $\tilde{H}_y$ on the left hand side of (4) is approximated at

$$\left.\frac{d\tilde{H}_y(t)}{dt}\right|_{t=n\Delta t} = \frac{\tilde{H}_y(n\Delta t + 0.5\Delta t) - \tilde{H}_y(n\Delta t - 0.5\Delta t)}{\Delta t}. \tag{6}$$

Besides, the convolution on the right hand side of (5) can be calculated as

$$\begin{aligned}&\left\{\left(\frac{d\tilde{H}_y(t)}{dt}\right) * \left(\sqrt{\frac{\mu}{\sigma\pi}}\frac{U(t)}{\sqrt{t}}\right)\right\}_{t=n\Delta t}\\ &= \sqrt{\frac{\mu}{\sigma\pi}}\sum_{m=1}^{n}\left[\tilde{H}_y(m\Delta t + 0.5\Delta t) - \tilde{H}_y(m\Delta t - 0.5\Delta t)\right] Z_{n-m}\end{aligned} \tag{7}$$

In the above, $Z_0 = \int_0^{1/2}(t')^{-1/2}dt' = \sqrt{2}$ and $Z_m = \int_{m-1/2}^{m+1/2}(t')^{-1/2}dt' = 2(\sqrt{m+1/2} - \sqrt{m-1/2})$, $m = 1, 2, 3, \ldots$ Substitution of (6) and (7) into (4) yields an update equation for $\tilde{H}_y$:

$$\begin{aligned}&\tilde{H}_y(n\Delta t + 0.5\Delta t) = \tilde{H}_y(n\Delta t - 0.5\Delta t)\\ &-\frac{\Delta t}{Q\Delta x}\sqrt{\frac{\mu}{\sigma\pi}}\sum_{m=1}^{n-1}\left[\tilde{H}_y(m\Delta t + 0.5\Delta t) - \tilde{H}_y(m\Delta t - 0.5\Delta t)\right] Z_{n-m}\\ &-\frac{\Delta t}{Q\Delta z}\left[E_x^U(n\Delta t) - E_x^L(n\Delta t)\right] - \frac{\Delta t}{Q\Delta x}E_z^L(n\Delta t)\end{aligned} \tag{8}$$

where $Q = \tilde{\mu} + Z_0\frac{\Delta t}{\Delta x}\sqrt{\frac{\mu}{\sigma\pi}}$. In the situation in Figure 2(b), both E_z^R and E_x^U are located on Γ hence they both should be obtained from $\tilde{H}_y$

through IBC. The update equation for $\tilde{H}_y$ is

$$\tilde{H}_y(n\Delta t + 0.5\Delta t) = \tilde{H}_y(n\Delta t - 0.5\Delta t)$$
$$-\frac{\Delta t}{Q_1}\left(\frac{1}{\Delta x}+\frac{1}{\Delta z}\right)\sqrt{\frac{\mu}{\sigma\pi}}\sum_{m=1}^{n-1}\left[\tilde{H}_y(m\Delta t+0.5\Delta t)-\tilde{H}_y(m\Delta t-0.5\Delta t)\right]Z_{n-m}$$
$$+\frac{\Delta t}{Q_1\Delta z}E_x^L(n\Delta t) - \frac{\Delta t}{Q_1\Delta x}E_z^L(n\Delta t) \tag{9}$$

where $Q_1 = \tilde{\mu} + Z_0\Delta t\left(\frac{1}{\Delta x}+\frac{1}{\Delta z}\right)\sqrt{\frac{\mu}{\sigma\pi}}$. Clearly, Equation (9) can be extended to all scenarios in which $\tilde{\mathbf{r}}$ is located next to an edge of Γ, and Equation (8) can be applied when $\tilde{\mathbf{r}}$ is next to Γ but not next to an edge of Γ. Since Γ is an enclosed surface, no other boundary conditions are necessary in our FDTD simulator. The summations over m in (8) and (9) are computationally expensive. To be more serious, they make load balancing in subsequent parallelization a difficult task since the boundary samples require much more computations than interior samples. To resolve this difficulty, "matrix pencil" technique in [12] is utilized to represent Z_m as superposition of a few exponential terms

$$Z_m = \sum_{l=1}^{L}\alpha_l e^{j\beta_l m}, \quad m = 1, 2, 3, \ldots, \tag{10}$$

where the coefficients $\{\alpha_l, \beta_l\}$ can be obtained from the algorithm in [12] with $\{Z_m\}$ as the input. As a result of (10), the summations over m in (8) and (9) can be evaluated as

$$\sum_{m=1}^{n-1}\left[\tilde{H}_y(m\Delta t + 0.5\Delta t) - \tilde{H}_y(m\Delta t - 0.5\Delta t)\right]Z_{n-m} = \sum_{l=1}^{L}\Phi_l^n, \tag{11}$$

where Φ_l^n is updated iteratively at each time step,

$$\Phi_l^n = \left\{\tilde{H}_y[(n-1)\Delta t+0.5\Delta t]-\tilde{H}_y[(n-1)\Delta t-0.5\Delta t]\right\}\alpha_l e^{j\beta_l} + e^{j\beta_l}\Phi_l^{(n-1)},$$
$$\text{with } \Phi_l^1 = \Phi_l^0 = 0 \tag{12}$$

Matrix pencil algorithm is chosen here to efficiently evaluate the discrete convolution in Equation (11), as it offers better accuracy than conventional algorithms like Prony's [13]. In this paper, $L = 15$ is enough to guarantee 10^{-3} relative accuracy in (10) for 100,000 time steps.

To facilitate MoM simulation of TR-UWB communication in metallic boxes, an equivalent problem is constructed as in Figure 3. The box wall is removed and exterior region is filled with free space

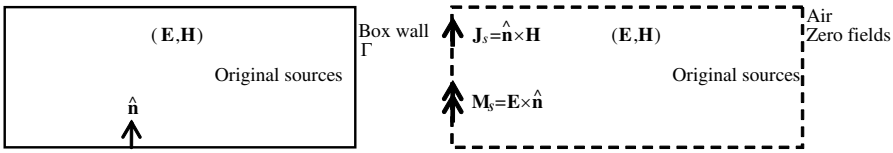

Figure 3. Illustration of MoM simulator.

and zero fields. Surface electric current $\mathbf{J}_s = \hat{\mathbf{n}} \times \mathbf{H}$ and magnetic current $\mathbf{M}_s = \mathbf{E} \times \hat{\mathbf{n}}$ reside on Γ. When box wall is made of good conductors, $\mathbf{M}_s$'s contribution is negligible, hence a simple integral equation is constructed:

$$\hat{\mathbf{n}}(\mathbf{r}) \times \hat{\mathbf{n}}(\mathbf{r}) \times \left[\mathbf{E}^{sca}(\mathbf{r}) + \mathbf{E}^{inc}(\mathbf{r})\right] = -Z_s \mathbf{J}_s(\mathbf{r}) = -\sqrt{\frac{j\omega\mu}{\sigma}}\mathbf{J}_s(\mathbf{r}), \quad (13)$$

where incident field $\mathbf{E}^{inc}$ and scattered field $\mathbf{E}^{sca}$ are produced by original sources in the box and surface current $\mathbf{J}_s$, respectively. Rao-Wilton-Glisson basis functions are used to discretize $\mathbf{J}_s$, and MoM matrix results from Galerkin testing [14]. Compared to regular electric field integral equations in [14], there is only one additional term on the right hand side of (13), and it can be straightforwardly incorporated into the MoM matrix. The MoM matrix is then inverted by LU decomposition. As a direct inversion algorithm, LU decomposition is preferred here since the resonant geometry in Figure 3 makes it very hard for iterative algorithms to converge.

Both the FDTD and MoM solvers are implemented on parallel cluster computers with distributed memory, to relieve high computational resources requirements. In the parallel FDTD solver, the Yee grids are partitioned into $P_x \times P_y \times P_z$ blocks along x, y, and z directions, and each processor is in charge of one block [15]. Information exchange occurs across the boundaries of adjacent blocks. To parallelize the MoM solver, the discrete unknowns are evenly distributed into multiple processors. No communication is necessary when the MoM matrix is filled, and the matrix is inverted with the aid of a parallel LU decomposition program. Message passing interface is adopted in all of our parallel implementation [16].

3. NUMERICAL RESULTS

Two numerical examples are presented in this section to demonstrate TR-UWB technique in metallic boxes.

In the first example, the metallic box is an empty cube with side length 0.33 m as shown in the inset of Figure 4. An RX and a TX are located at (0.165 m, 0.135 m, 0.165 m) and (0.165 m, 0.24 m, 0.165 m), respectively. Both RX and TX are assumed small dipoles oriented

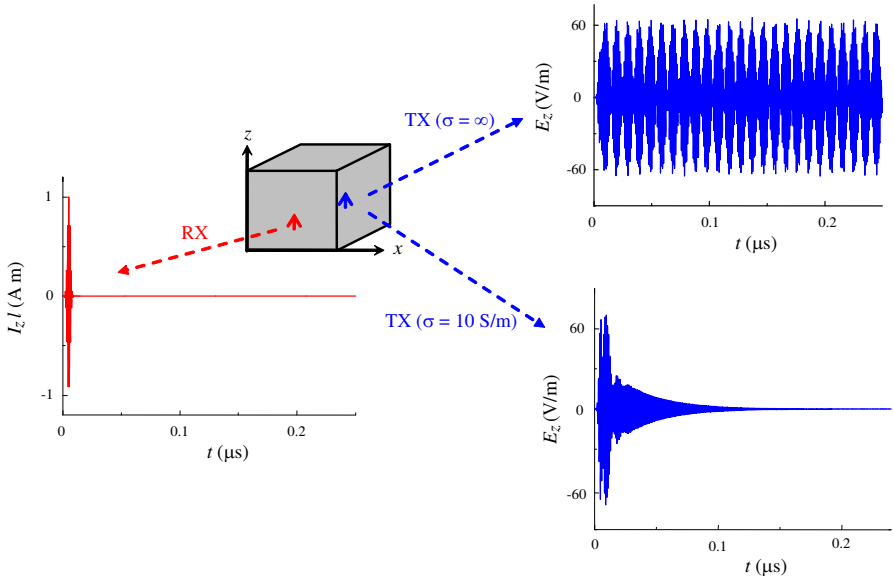

Figure 4. Numerical results for backward propagation (RX to TX) in a cubic box.

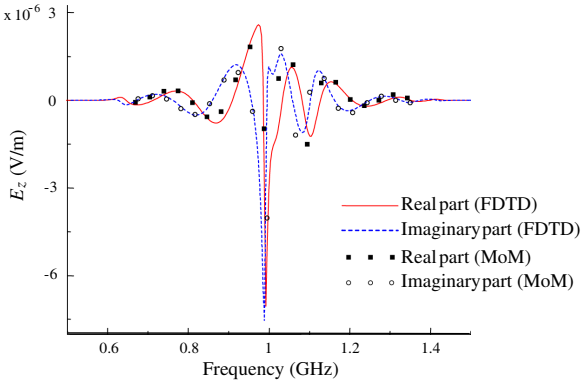

Figure 5. Electric field signal received at TX in Figure 4 (when $\sigma = 10\,\mathrm{S/m}$).

along z direction. During backward propagation, the signal at RX is

$$I_z l = \cos[2\pi f_0(t - t_0)]e^{-(t-t_0)^2/(2\tau^2)} \text{ (Am)}, \tag{14}$$

with $f_0 = 1\,\text{GHz}$, $\tau = 1.2\,\text{ns}$, and $t_0 = 5\tau$. Source waveform at the RX and electric field received at the TX (from FDTD simulator) are plotted in Figure 4. Unsurprisingly, when the box wall is assumed to be made of perfect conductor, the received electric field is endless in time due to infinite number of multiple reflections. When the conductivity of box wall is $10\,\text{S/m}$, the received signal is attenuated in time by the imperfection of box wall. In Figure 5, the signals received at TX obtained by FDTD and MoM solvers when $\sigma = 10\,\text{S/m}$ are compared to one another, and excellent agreement is observed. Next, when $\sigma = 10\,\text{S/m}$, the TX time reverses the signal that it receives at the backward propagation stage and transmits the reserved signal to the RX. The transmitted waveform at TX and electrical field received at the RX are plotted in Figure 6. Clearly, a short impulse is observed at the RX (temporal compression). Contrast between this impulse and the rest in time gets even sharper with the increase of σ. Thanks to the high contrast, the impulse can be easily detected by simple non-coherent receiver circuitries.

In the second example, the metallic box is of "L" shape and filled with air, as depicted in the inset of Figure 7. The conductivity of the box walls is $10\,\text{S/m}$. An RX and a TX, which are small z-orientated dipoles, are located at $(0.1\,\text{m}, 0.4\,\text{m}, 0.2\,\text{m})$ and $(0.4\,\text{m}, 0.05\,\text{m}, 0.2\,\text{m})$, respectively (note that the RX and TX do not have line-of-sight interactions). Round-trip propagation similar to that in the first example is carried out. During backward propagation, an impulse is transmitted from the RX to the TX. The impulse's waveform is as that in (14), with $f_0 = 4.5\,\text{GHz}$, $\tau = 0.318\,\text{ns}$, and $t_0 = 6\tau$. As expected, the

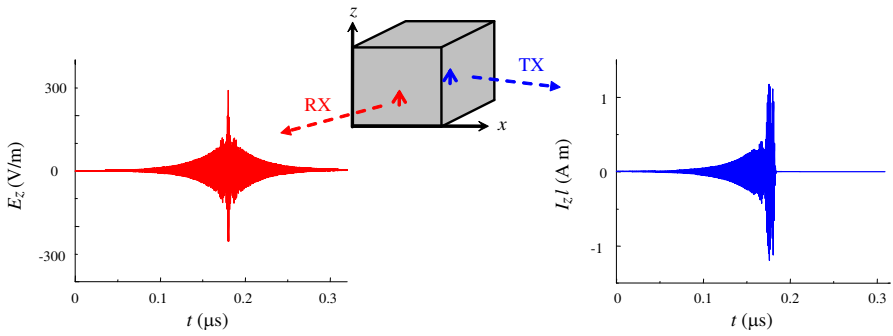

Figure 6. Numerical results for forward propagation (TX to RX) in a cubic box.

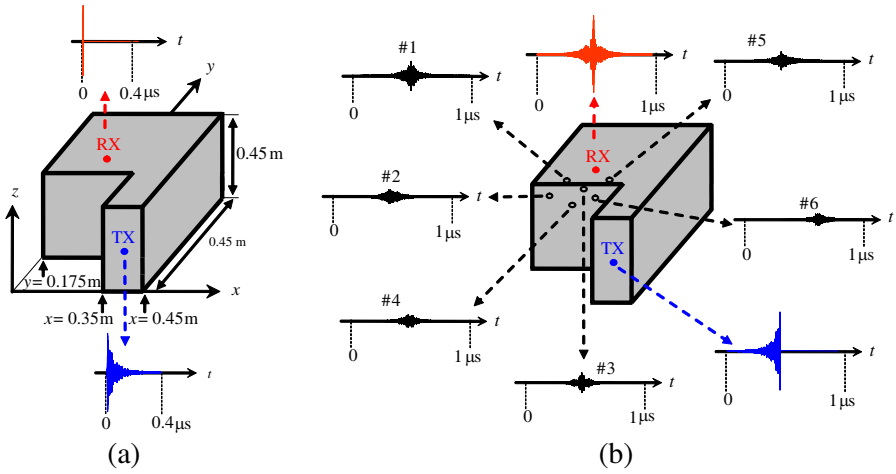

Figure 7. Numerical results for TR-UWB communication in an L-shaped box. (a) Backward propagation (from RX to TX). (b) Forward propagation (from TX to RX).

signal at the TX after backward propagation (in Figure 7(a)) consists of a long tail. After this signal is time reversed and transmitted by the TX though forward propagation, a narrow impulse is achieved at the RX (Figure 7(b)). In addition to temporal compression, spatial focusing is also exhibited in Figure 7(b). Six locations around the RX are picked with coordinates (0.05 m, 0.35 m, 0.2 m), (0.05 m, 0.25 m, 0.2 m), (0.1 m, 0.3 m, 0.2 m), (0.1 m, 0.2 m, 0.2 m), (0.15 m, 0.35 m, 0.2 m), and (0.15 m, 0.25 m, 0.2 m), respectively. Compared to the signal at the RX, electric fields at these six locations are much weaker.

4. CONCLUSIONS

In this paper, numerical studies are carried out to demonstrate feasibility of applying TR-UWB technique to wireless communication in boxes with metallic enclosure. Two parallel full-wave simulators (one based on FDTD and the other MoM) are developed, with metallic walls modeled by IBC. Focusing of electromagnetic waves on both space and time is exhibited by numerical results in arbitrarily shaped metallic boxes. Current research efforts include incorporating wide-band antenna models, which call for hybrid simulation of MoM and FDTD.

ACKNOWLEDGMENT

The authors would like to acknowledge Texas Advanced Computing Center (TACC) for granting access to its computational facilities.

REFERENCES

1. Hwu, S. U., Y.-C. Loh, and C. C. Sham, "Space station wireless local area network signal characteristics modeling and measurements," *2006 IEEE/AIAA 25th Digital Avionics Systems Conference*, Portland, Oregon, October 2006.
2. Niu, W., J. Li, and T. Talty, "Ultra-wideband channel modeling for intravehicle environment," *EURASIP Journal on Wireless Communications and Networking*, Vol. 2009, Article ID 806209, 12, 2009.
3. Van't Hof, J. P. and D. D. Stancil, "Characterizing dispersion in the enclosed-space radio channel using a composite mode model," *IEEE/ACES International Conference on Wireless Communications and Applied Computational Electromagnetics*, Honolulu, HI, April 2005.
4. Naqvi, I. H. and G. E. Zein, "Time domain measurements for a time reversal SIMO system in reverberation chamber and in an indoor environment," *IEEE International Conference on Ultra-wideband*, Hannover, Germany, September 2008.
5. Zhou, C., N. Guo, and R. C. Qiu, "Time-reversed ultra-wideband (UWB) multiple input multiple output (MIMO) based on measured spatial channels," *IEEE Transactions on Vehicular Technology*, Vol. 59, No. 6, 2884–2898, July 2009.
6. Win, M. Z. and R. A. Scholtz, "Characterization of ultra-wide bandwidth wireless indoor channels: A communication-theoretic view," *IEEE Journal on Selected Areas in Communications*, Vol. 20, No. 9, 1613–1627, 2002.
7. Oestges, C., A. D. Kim, G. Papanicolaou, and A. J. Paulrai, "Characterization of space-time focusing in time-reversed random fields," *IEEE Transactions on Antennas and Propagation*, Vol. 53, No. 1, 283–293, January 2005.
8. Wertz, P., D. Zimmermann, F. M. Landstorfer, G. Wolfle, and R. Hoppe, "Hybrid ray optical models for the penetration of radio waves into enclosed spaces," *58th IEEE Vehicular Technology Conference*, Orlando, FL, October 2003.
9. Yuferev, S. and N. Ida, "Selection of the surface impedance

boundary conditions for a given problem," *IEEE Transactions on Magnetics*, Vol. 35, No. 3, 1486–1489, May 1999.

10. Leontovich, M. A., "On the approximate boundary conditions for electromagnetic fields on the surface of well conducting bodies," *Investigations of Propagation of Radio Waves*, 2–20, 1948.
11. Taflove, A. and S. C. Hagness, *Computational Electrodynamics: The Finite-difference Time-domain Method*, Artech House, Norwood, MA, 2005.
12. Hua, Y. and T. K. Sarkar, "Matrix pencil method for estimating parameters of exponentially damped/undamped sinusoids in noise," *IEEE Transactions on Acoustics, Speech, and Signal Processing*, Vol. 38, No. 5, 814–824, 1990.
13. Beggs, J. H., R. J. Luebbers, K. S. Yee, and K. S. Kunz, "Finite-difference time-domain implementation of surface impedance boundary conditions," *IEEE Transactions on Antennas and Propagation*, Vol. 40, No. 1, 49–56, January 1992.
14. Rao, S. M., D. R. Wilton, and A. W. Glisson, "Electromagnetic scattering by surfaces of arbitrary shape," *IEEE Transactions on Antennas and Propagation*, Vol. 30, No. 3, 409–418, May 1982.
15. Yu, W., R. Mittra, T. Su, Y. Liu, and X. Yang, *Parallel Finite-difference Time-domain Method*, Artech House, Norwood, MA, 2006.
16. Gropp, W., E. Lusk, and A. Skjellum, *Using MPI: Portable Parallel Programming with the Message-passing Interface*, 2nd edition, MIT Press, Cambridge, MA, 1999.